nature materials

ARTICLES

PUBLISHED ONLINE: 4 SEPTEMBER 2011 | DOI: 10.1038/NMAT3104

Gas detection by structural variations of fluorescent guest molecules in a flexible porous coordination polymer

Nobuhiro Yanai[1], Koji Kitayama[1], Yuh Hijikata[1], Hiroshi Sato[2,3], Ryotaro Matsuda[2,3], Yoshiki Kubota[4], Masaki Takata[5], Motohiro Mizuno[6], Takashi Uemura[1]* and Susumu Kitagawa[1,2,3]*

The development of a new methodology for visualizing and detecting gases is imperative for various applications. Here, we report a novel strategy in which gas molecules are detected by signals from a reporter guest that can read out a host structural transformation. A composite between a flexible porous coordination polymer and fluorescent reporter distyrylbenzene (DSB) selectively adsorbed CO_2 over other atmospheric gases. This adsorption induced a host transformation, which was accompanied by conformational variations of the included DSB. This read-out process resulted in a critical change in DSB fluorescence at a specific threshold pressure. The composite shows different fluorescence responses to CO_2 and acetylene, compounds that have similar physicochemical properties. Our system showed, for the first time, that fluorescent molecules can detect gases without any chemical interaction or energy transfer. The host–guest coupled transformations play a pivotal role in converting the gas adsorption events into detectable output signals.

Recently, luminescence gas sensors have attracted considerable attention for a wide variety of applications, because the sensing output is visible to the naked eye, which allows on-site and instantaneous decision-making even in explosive and flammable locations and complex environments[1–3]. There have been many examples of gas detection that use luminescence quenching by energy transfer between gases and luminescent materials[4,5]. However, only a limited number of gases, such as O_2 and NO_2, can induce such quenching, and it is difficult to attain sensitive monitoring with the quenching mechanism[6]. A few materials have offered gas detection with luminescence colour switching or turn-on switching properties by chemical interactions and reactions, which have problems such as responsivity to only a single specific (reactive) gas, solution-containing device, difficulty in reuse, and slow response[7–9]. These problems can be overcome by the construction of a gas detection system that responds precisely and quickly to weaker interactions such as physical adsorption. However, there has been no strategy to achieve luminescence materials that can read out such weak interactions.

Porous coordination polymers (PCPs) or metal organic frameworks (MOFs) have emerged as particularly exciting solid porous materials[10–14], and they offer a wide range of potential applications, such as gas storage, separation, catalysis, sensing and drug delivery[15–23]. The size, shape, and surface functionality of pores can be controlled through the proper combination of organic ligands and metal ions. Compared with conventional porous materials, one of the most intriguing advantages of PCPs is their flexible frameworks[11,15,21,24–26]. This structural flexibility, causing a structural transformation from a closed form to an open form, is the key factor for the selective uptake of target gas molecules by recognizing small differences in their physicochemical properties.

Our strategy to achieve gas detection includes the accommodation of a reporter molecule that can read out structural transformations of a flexible PCP (Fig. 1). The obtained composite material can further adsorb gas molecules as a second guest, providing a 'co-adsorption state'. The structural transformation of PCPs on gas adsorption results in a dynamic change in the pore size and shape with adjusting host–guest interactions, which will alter the conformations of the reporter molecule. Such conformational variations of the reporter molecule can lead to different output signals, where the adsorbed gas molecules will be successfully detected. Although many types of host–guest materials have been reported, there have been few examples in which host structural transformations affect not only the guest structures but also the guest properties[27].

This strategy has several advantages for effective gas detection. The flexible PCPs entrap reporter molecules by changing the pore structures to maximize the host–guest interactions; thus, the obtained composites are closed forms. Such composites would selectively adsorb gases for which interactions with the composites were strong enough to change the framework structures from closed to open forms[28]. A gate effect often occurs during such a gas adsorption process involving framework transformations, which generates abrupt adsorptions at particular threshold pressures[11,15,21,24–26]. Thus, the specific gases and their pressures can be monitored by the change in output from the reporter molecules. In addition, there are diverse combinations of flexible PCPs and reporter molecules, which expands the versatility and possibility of gas detection.

[1]Department of Synthetic Chemistry and Biological Chemistry, Graduate School of Engineering, Kyoto University, Katsura, Nishikyo-ku, Kyoto 615-8510, Japan, [2]ERATO Kitagawa Integrated Pores Project, Japan Science and Technology Agency (JST), Kyoto Research Park Bldg #3, Shimogyo-ku, Kyoto, 600-8815, Japan, [3]Institute for Integrated Cell-Material Sciences (iCeMS), Kyoto University, Yoshida, Sakyo-ku, Kyoto 606-8501, Japan, [4]Department of Physical Science, Graduate School of Science, Osaka Prefecture University, Sakai, Osaka 590-0035, Japan, [5]Structural Materials Science Laboratory, Harima Institute, RIKEN SPring-8 Center and CREST, JST, Sayo-gun, Hyogo, 679-5148, Japan, [6]Department of Chemistry, Graduate School of Natural Science and Technology, Kanazawa University, Kanazawa 920-1192, Japan. *e-mail: uemura@sbchem.kyoto-u.ac.jp; kitagawa@icems.kyoto-u.ac.jp.

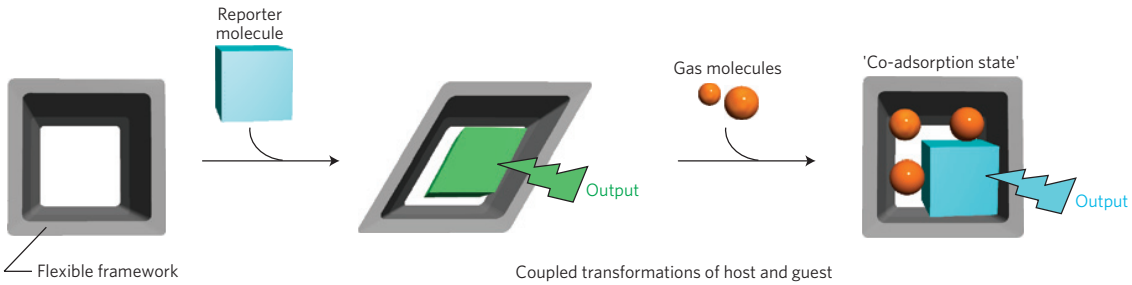

Figure 1 | Schematic illustration for detection of gas molecules by coupled structural transformations of a flexible PCP framework and a reporter molecule. The induced-fit-type structural change of the flexible PCP framework occurs by inclusion of a reporter molecule. The subsequent structural transformation of PCP during the gas adsorption process leads to a large change of pore structure. This is accompanied by the conformational variations of the reporter molecule, which leads to the change of output signal.

In this paper, we demonstrate the luminescence detection of gas molecules by means of coupled transformations of a flexible PCP and a fluorescent reporter molecule, distyrylbenzene (DSB). It has been reported that the conformational variations of DSB and its derivatives lead to large changes in their fluorescence properties[29–31]. We introduced the DSB molecules into nanochannels of a flexible host compound $[Zn_2(terephthalate)_2(triethylenediamine)]_n$ (**1**; channel size = 7.5 × 7.5 Å^2) in which two-dimensional (2D) square grids are bridged by triethylenediamine[32]. The obtained PCP–DSB composite material selectively adsorbed CO_2 over other atmospheric gases, such as N_2, O_2, and Ar. Interestingly, during the adsorption process of CO_2, the conformation of DSB varied concurrently with an expansion of the host framework, which resulted in a critical response for the DSB fluorescence at a particular threshold pressure. In addition, the PCP–DSB composite can distinguish two gases with similar physicochemical properties, CO_2 and acetylene (C_2H_2), by means of different luminescence outputs. Taking advantage of the structural flexibility of the PCP, the PCP–DSB composite system showed the first example of gas detection by a fluorescence change in organic molecules without any chemical interaction or energy transfer. The unique detection methodology based on host–guest co-operativity would create new possibilities for the development of advanced detection systems.

Introduction of DSB into the nanochannels of **1** was conducted at 503 K by the sublimation method (Fig. 2)[33]. X-ray powder diffraction (XRPD) measurement showed that the introduction of DSB induced a significant change in the host structure, which confirms the formation of the host–guest composite (Supplementary Fig. S1). The deformed host framework is denoted by **1**′, and the composite is described as **1**′ ⊃ DSB. The crystals of the host PCP did not collapse during the loading process with DSB, as shown by scanning electron microscope measurements (Supplementary Fig. S2). Elemental analysis of **1**′ ⊃ DSB showed that the number of DSB molecules per unit cell of the host was 0.81. The XRPD pattern of **1**′ ⊃ DSB is similar to that of the compound obtained by introducing benzene into **1**, in which the overall framework connectivity remains similar to **1**, but the square grid structure is distorted to form a rhombic net (Supplementary Table S1)[32]. The results of a Le Bail fitting analysis of the synchrotron XRPD data of **1**′ ⊃ DSB showed that the introduction of DSB induced a large distortion of the 2D net (the angle between sides of the 2D net is 75°; Supplementary Fig. S3, Table S1). The distances between the two neighbouring dinuclear Zn_2 units are almost the same as those in guest-free **1**, but the volume per Zn_2 unit is smaller (1,078 Å^3) than that for **1** (1,148 Å^3). Thus, the inclusion of DSB resulted in shrinkage of the host framework.

Infrared and Raman spectroscopy showed that the conformation of DSB was changed by being included within the host nanochannels. The infrared spectrum of bulk DSB has a few peaks around 970 cm^{-1} that are assignable to a CH out-of-plane bending vibration of the CH = CH groups (Supplementary Fig. S4)[34]. When DSB was incorporated into the nanochannels, these peaks clearly shifted to 954 cm^{-1}. Density functional calculations showed that the corresponding infrared band shifts to lower wavenumbers with increasing torsional angles around the C = C and C–phenyl bonds (Supplementary Fig. S5)[34]. As suggested by this trend, the conformation of DSB in the bulk crystals is almost planar, whereas that in the rhombic channels of **1**′ is twisted. Raman measurements also supported the twisted conformation of DSB in **1**′ (Supplementary Fig. S6). The ultraviolet–visible absorption spectrum of **1**′ ⊃ DSB showed a red shift compared with that of DSB in solution because of the formation of *J*-aggregates of DSB in **1**′ (Supplementary Fig. S7)[29,35,36].

The composite **1**′ ⊃ DSB could adsorb further gases as second guests by means of the breathing mechanism[25]. As for atmospheric gases, whereas the composite **1**′ ⊃ DSB did not adsorb N_2, O_2 or Ar, it could selectively adsorb CO_2 in a stepwise fashion (Fig. 3a). In this open-gate-type adsorption, flexible PCPs can distinguish gases according to subtle differences such as quadrupole moments and clathrate formation. CO_2 has a larger quadrupole moment ($13.4 \times 10^{40}\theta$ C^{-1} m^{-2}) than those of N_2 ($4.7 \times 10^{40}\theta$ C^{-1} m^2), O_2 ($1.3 \times 10^{40}\theta$ C^{-1} m^2), and Ar (0θ C^{-1} m^2; ref. 37). The co-operative clathrate formation of CO_2 would also contribute to the selective CO_2 uptake[38,39]. The CO_2 adsorption isotherm shows a sharp increase at low pressures (up to point A, where P = 1 kPa). After reaching point B (P = 28 kPa), the isotherm exhibited another sharp increase, and finally attained a saturated level (5.0 molecules per 1 unit) at point C (P = 96 kPa). To examine the host structure and guest conformation during the stepwise adsorption, we carried out *in situ* XRPD and infrared measurements with an increase in CO_2 pressure at 195 K (Fig. 3b,c). From the XRPD patterns in the region from 30 to 60 kPa of CO_2 pressure, the deformed (**1**′) and original (**1**) host structures coexisted, with the amount of the former decreasing as the latter increased. At P = 80 kPa, the original structural phase of **1** was dominant. The infrared band of the CH out-of-plane vibration showed an upward shift above a CO_2 pressure of 30 kPa, indicating the conformational planarization of DSB. From these results, the shrunk rhombic structure of **1**′ ⊃ DSB was expanded to the original square form at the specific pressure of CO_2, which was accompanied by alteration of the DSB conformation. Note that the removal of the adsorbed CO_2 by vacuuming regenerated the host structure and DSB conformation of **1**′ ⊃ DSB.

Remarkably, the solid-state fluorescence of the composite material presented a critical response towards CO_2 adsorption. Under ultraviolet irradiation, the composite **1**′ ⊃ DSB produced a weak green fluorescence at 195 K (Fig. 2). On the other hand,

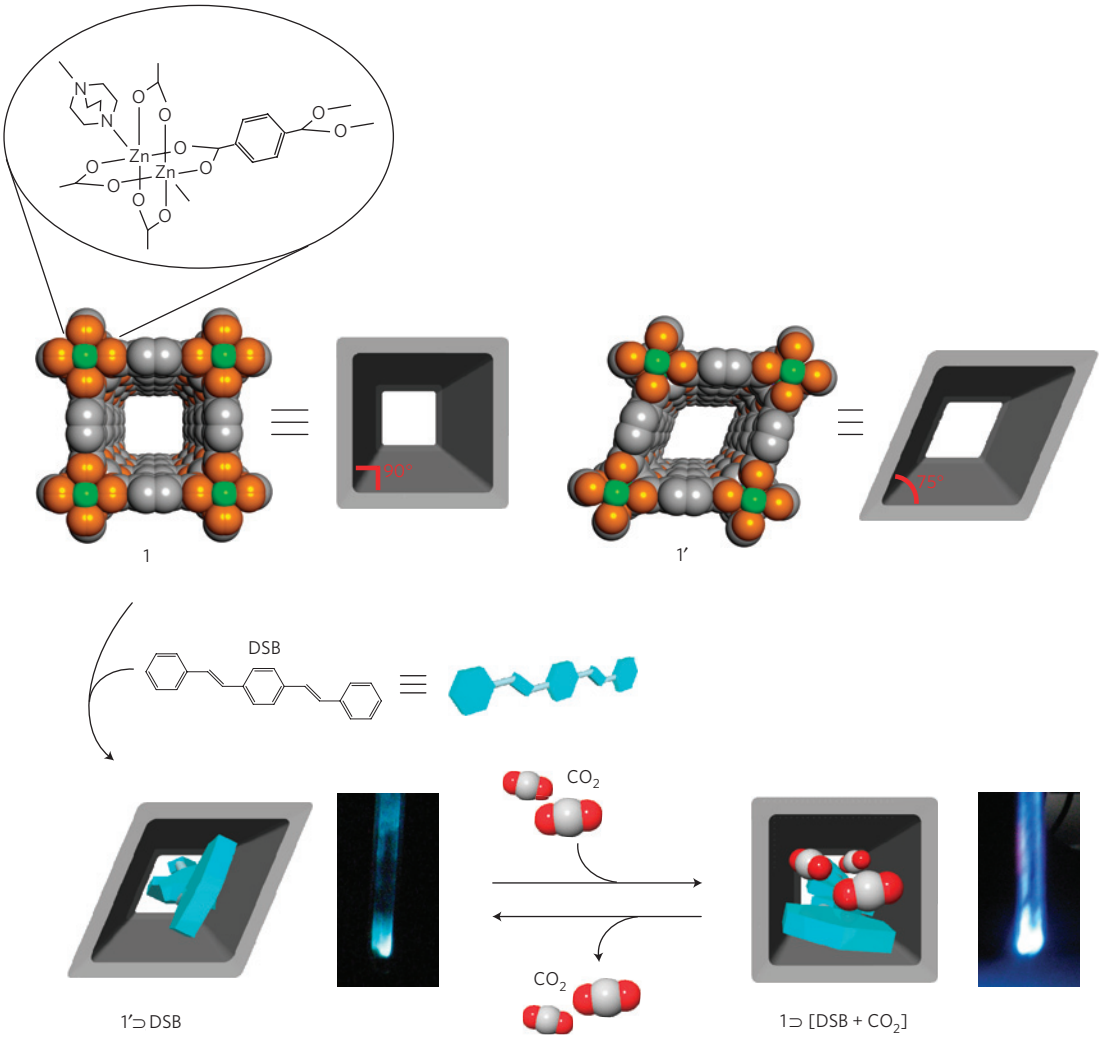

Figure 2 | Introduction of reporter molecule DSB into flexible host 1, and structural and fluorescence changes of the composite by co-adsorption of CO_2. The original and deformed host structures are denoted as **1** and **1′**, respectively. The adsorption of CO_2 on **1′** ⊃ DSB induces the coupled changes of the PCP structure and DSB conformations, resulting in the critical fluorescence response towards CO_2. Pictures of the composite materials were taken at 195 K under ultraviolet irradiation (excitation at 366 nm). The removal of CO_2 from **1** ⊃ [DSB + CO_2] by vacuuming at 195 K regenerates the original composite **1′** ⊃ DSB.

a clear blue fluorescence was observed from the composite on introducing CO_2 gas at 195 K. The fluorescence colour change started within a few seconds, and was complete within a few minutes. Figure 3d shows the fluorescence spectra of **1′** ⊃ DSB under different CO_2 pressures. The fluorescence spectrum of **1′** ⊃ DSB under vacuum was broad, which may be explained by hindrance of the relaxation process from the twisted state to the planar excited state[30,40]. The spectra changed markedly and featured vibronic structures above a specific threshold pressure ($P = 30$ kPa) that corresponds to the step of the adsorption isotherm. The appearance of vibronic spectra is attributable to the planarization of the DSB molecules[30,40]. Although conformational planarization usually extends the effective π-conjugation length of molecules, the excitation and fluorescence spectra showed a slight blue shift after CO_2 uptake, which is probably because of the alteration of the aggregation structure of DSB (Fig. 3d and Supplementary Fig. S8)[29,30,35]. The original guest fluorescence of **1′** ⊃ DSB was regenerated by removing CO_2 from the composite **1** ⊃ [DSB+CO_2], confirming the easy reuse of the detection system. Note that the shape and position of the fluorescence spectrum of **1′** ⊃ DSB was not affected by N_2, O_2, and Ar (Supplementary Fig. S9); thus, the composite selectively sensed CO_2 among the atmospheric gases. Furthermore, the particular threshold pressure was detected by a clear change in the solid-state fluorescence. This type of detection is important for quality control to ensure the proper functions of CO_2-containing gases in industrial processes, and to safeguard against their waste streams into the atmosphere[8]. Notably, the DSB fluorescence in rigid PCPs was not sensitive to CO_2, which highlights the importance of the framework transformation for the fluorescence response (Supplementary Fig. S10).

Flexible PCPs can also differentiate gases with similar properties, which allows fluorescence detection of these gases. We employed CO_2 and C_2H_2 as target gases because it is important to distinguish C_2H_2 from CO_2 in the production and use of C_2H_2; however, this differentiation is difficult because of their similar physicochemical properties (Supplementary Table S2)[41–43]. The adsorption isotherm of C_2H_2 for **1′** ⊃ DSB shows a steep rise in the low-pressure region and reaches saturation, which is very different from the stepwise isotherm of CO_2 (Fig. 4a). The observed difference might be due to the stronger interaction of C_2H_2 with the pore walls than that of CO_2. The pore walls are mainly composed of aromatic and aliphatic moieties, but there are negatively polarized oxygen atoms of carboxylate ligands that can form attractive electrostatic interactions with the positively polarized hydrogen atoms of

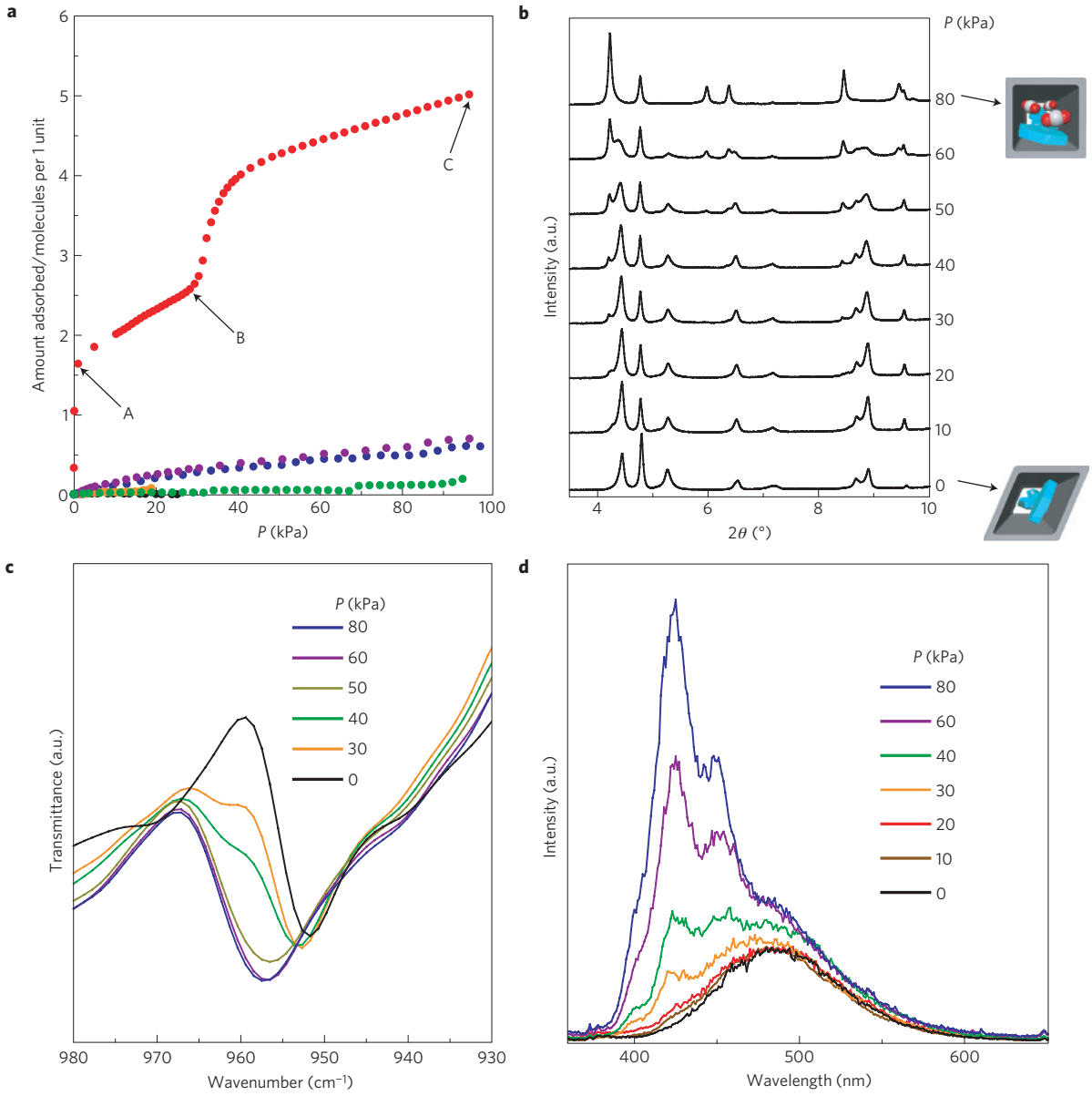

Figure 3 | Selective adsorption of CO_2 among atmospheric gases, and the changes of host structure, guest conformation, and fluorescence at the specific pressure of CO_2. **a**, Adsorption isotherms of CO_2 (red), N_2 (blue), and O_2 (purple) at 195 K, and of N_2 (green), O_2 (orange), and Ar (black) at 77 K on **1**′ ⊃ DSB. **b**, *In situ* synchrotron XRPD patterns with increasing pressure of CO_2 for **1**′ ⊃ DSB at 195 K. Schematic representations of the composites are also shown. **c**, *In situ* infrared spectra with increasing pressure of CO_2 for **1**′ ⊃ DSB at 195 K. **d**, *In situ* fluorescence spectra (excitation at 340 nm) with increasing pressure of CO_2 for **1**′ ⊃ DSB at 195 K.

C_2H_2 (refs 41,44,45). The larger quadrupole moment of C_2H_2 ($20.4 \times 10^{40}\theta\ C^{-1}\ m^{-2}$) than that of CO_2 ($13.4 \times 10^{40}\theta\ C^{-1}\ m^{-2}$) may also contribute to the larger electrostatic interaction of C_2H_2 with the host framework[37,41,44]. From *in situ* XRPD and infrared measurements, the structural transformation of the host framework was complete at even at low pressures of C_2H_2 ($P = 5.0$ kPa), which is accompanied by the conformational planarization of DSB (Fig. 4b,c). Thus, the solid-state fluorescence of the composite showed a clear change at $P = 7.0$ kPa (Fig. 4d). In contrast to this, no fluorescence response was observed below the threshold CO_2 pressure of 30 kPa (Fig. 3d). From these results, the two gases, C_2H_2 and CO_2, can be distinguished by monitoring the solid-state fluorescence. Compared with previously reported luminescence sensors, our detection system provides notable advantages, such as multiple-gas detection, solid-state sensing, fast response, easy reuse, and threshold-pressure monitoring. Control of the conformation and arrangement of the luminescent molecules in the solid state by external stimuli, such as heat, pressure, and recrystallization with solvents, has recently been proposed as an efficient mechanism for a luminescence switch[36,46–48]. We have demonstrated here the first example of such luminescence switching by gas adsorption.

To characterize the detailed mechanism of the fluorescence detection, we performed adsorption of solvent vapours into **1**′ ⊃ DSB. Water vapour cannot be adsorbed by **1**′ ⊃ DSB unless the vapour pressure is high ($P/P_0 > 0.7$; Supplementary Fig. S11). The fluorescence of **1**′ ⊃ DSB was not affected by water vapour below $P/P_0 = 0.67$; thus, the fluorescent detection performance would not be influenced by water (Supplementary Fig. S12). Meanwhile, the composite **1**′ ⊃ DSB readily adsorbs polar and non-polar organic molecules because of the hydrophobic nature of the pores (Supplementary Figs S13–S16). We employed polar molecules, such

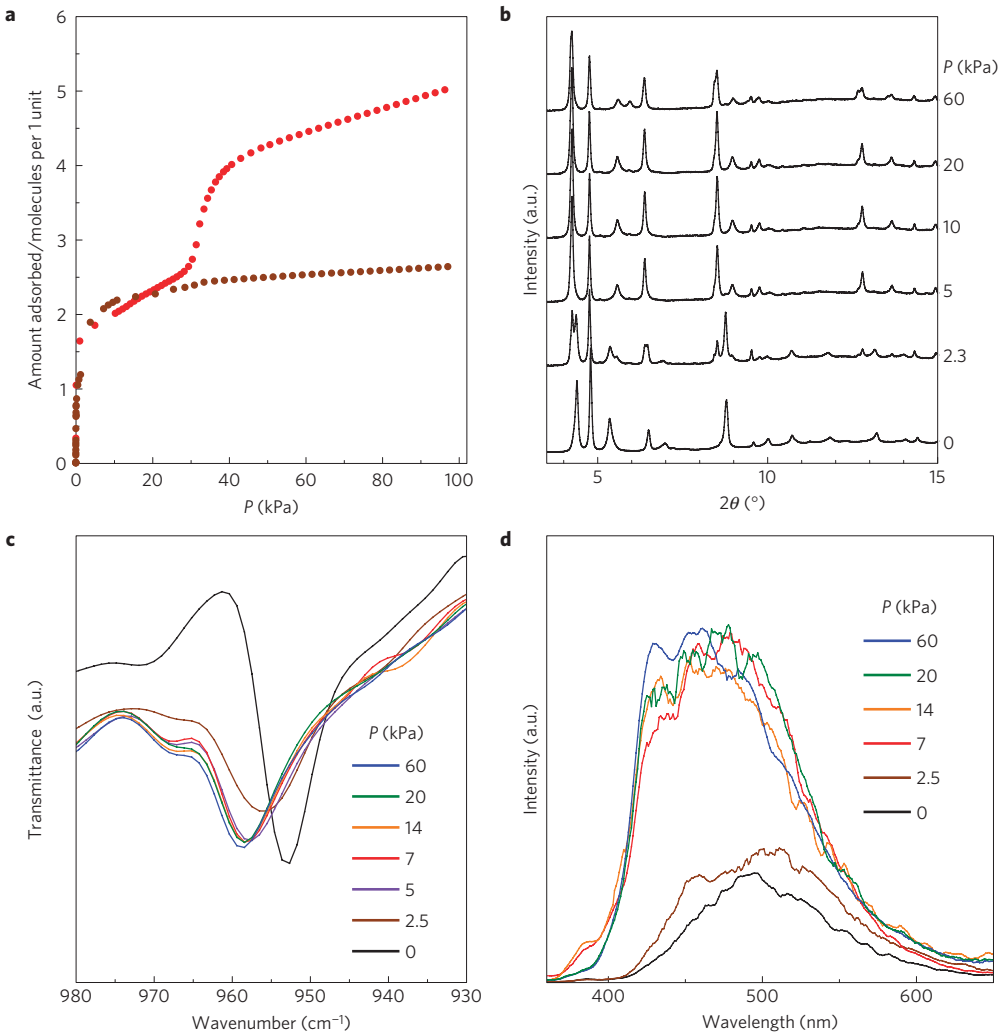

Figure 4 | Differentiation and fluorescence detection of multiple gases, CO_2 and C_2H_2, that have similar physicochemical properties. a, Adsorption isotherms of CO_2 (red) and C_2H_2 (brown) at 195 K on **1**′ ⊃ DSB. The isotherms show that the adsorption amount of C_2H_2 is smaller (2.6 molecules per 1 unit at $P = 97$ kPa) than that of CO_2 (5.0 molecules per 1 unit at $P = 96$ kPa). **b**, *In situ* synchrotron XRPD patterns with increasing pressure of C_2H_2 for **1**′ ⊃ DSB at 195 K. The host structure was not fully transformed to the original square grid structure **1** during C_2H_2 adsorption. The observed differences in the XRPD and adsorption measurements during CO_2 and C_2H_2 adsorptions might be due to the stronger interaction of the pore walls with C_2H_2 than that with CO_2. The stronger host–guest interaction allows the host structural change in the low-pressure region of C_2H_2, and stabilizes the C_2H_2-included structure, which prevents further adsorption of C_2H_2. **c**, *In situ* infrared spectra with increasing pressure of CO_2 for **1**′ ⊃ DSB at 195 K. **d**, *In situ* fluorescence spectra (excitation at 340 nm) with increasing pressure of CO_2 for **1**′ ⊃ DSB at 195 K.

as MeCN, MeOH, and acetone, as the second guest to avoid the release of DSB from the nanochannels. For example, the composite material **1**′ ⊃ DSB showed a stepwise adsorption of MeCN (Supplementary Fig. S16). The fluorescence intensity gradually increased in the course of the MeCN adsorption, which allows monitoring of the vapour pressure by the fluorescence intensity (Supplementary Fig. S17). After the second uptake of MeCN ($P/P_0 > 0.50$), structured fluorescence spectra were observed. The fluorescence quantum yield of the MeCN-filled sample **1** ⊃ [DSB + MeCN] was found to be 0.61, which is about 30 times higher than that of **1**′ ⊃ DSB (Table 1). As indicated by *in situ* XRPD and infrared measurements for **1**′ ⊃ DSB, the stepwise structural transformation of the host was accompanied by the gradual conformational planarization of DSB (Supplementary Figs S18 and S19). The fluorescence of DSB derivatives with bulky substituents was largely suppressed because of non-radiative deactivation induced by the twisted conformation with torsional angles of 20°–50° (ref. 30). Likewise, the planarization of the DSB molecules should contribute to an increase in the fluorescence intensity during the adsorption of the second guests. The fluorescence lifetimes of **1**′ ⊃ DSB (1.4 ns) and **1** ⊃ [DSB + MeCN] (2.0 ns) are comparable to that of DSB in solution, suggesting the absence of guest–guest excimer and host–guest exciplex complexes with long lifetimes (Table 1)[46,49].

Interestingly, the removal of MeCN from **1** ⊃ [DSB + MeCN] by vacuuming at 273 K provided a fluorescent solid **1** ⊃ DSB, with a host structure which remained the same as **1** (Supplementary Fig. S1). Thermal gravimetric analysis and solid-state ^{13}C NMR measurements affirmed the complete removal of MeCN (Supplementary Figs S20 and S21). The position of the infrared band and the Raman activity of the CH = CH group for **1** ⊃ DSB were almost identical to those for **1** ⊃ [DSB + MeCN], indicating the planar DSB conformation after removing MeCN (Supplementary Figs S6 and S19). In addition, the fluorescence spectrum, quantum yield, and lifetime of **1** ⊃ DSB were essentially the same as those of **1** ⊃ [DSB + MeCN] (Table 1 and Supplementary Fig. S22). Thus, the adsorbed molecules are not influential in the fluorescence of DSB in **1**, and the DSB fluorescence essentially depends on the

Table 1 | Fluorescence quantum yields and lifetimes for 1′ ⊃ DSB, 1 ⊃ [DSB + MeCN], 1 ⊃ DSB, and DSB solution at 298 K.

	Quantum yield	Lifetime (ns)
1′ ⊃ DSB	0.02	1.4
1 ⊃ [DSB + MeCN]	0.61	2.0
1 ⊃ DSB	0.54	2.1
DSB in hexane	0.90*	1.4

*From ref. 30.

host structure. It is interesting that the composite material has a unique 'memory effect' after the removal of MeCN (Supplementary Fig. S13), which was not observed after the removal of CO_2 from **1** ⊃ [DSB + CO_2] (Fig. 2). The origin of these different behaviours might be explained by the different DSB conformations after the CO_2 and MeCN adsorptions (Supplementary Fig. S13). The differential scanning calorimetry (DSC) curve for **1** ⊃ DSB exhibited an exothermic peak around 403 K (Supplementary Fig. S23). The second DSC run showed no exotherm, which indicates an irreversible transition after the thermal treatment. The composite **1** ⊃ DSB was converted to **1**′ ⊃ DSB by heating at 423 K, as shown by the XRPD measurements (Supplementary Fig. S1). Furthermore, **1** ⊃ DSB slowly relaxed to **1**′ ⊃ DSB at room temperature over several months (Supplementary Fig. S24). The composites **1**′ ⊃ DSB and **1** ⊃ DSB are thus shown to be the thermodynamically and kinetically stable phases, respectively. The differences in host–guest interactions between **1**′ ⊃ DSB and **1** ⊃ DSB are reflected not only in the DSB conformation but also in the DSB mobility shown in the solid-state ^{2}H NMR measurements (Supplementary Fig. S25). The guest DSB confined in **1**′ was strongly constrained, whereas that in **1** had a higher mobility. The higher mobility of fluorescent molecules usually leads to a lower quantum yield; thus, the different DSB conformations in **1**′ ⊃ DSB and **1** ⊃ DSB would be the main cause of the fluorescence change[48]. After heating **1** ⊃ DSB, the DSB fluorescence also varied to that of **1**′ ⊃ DSB (Supplementary Fig. S22). Therefore, the DSB fluorescence was reversibly changed in response to the different host structures, which confirms the scenario that host–guest-coupled transformations play a key role in the fluorescence changes.

This work establishes a novel strategy for the capture and detection of gases by co-operative structural transformations of a flexible PCP and fluorescent reporter molecules. Interestingly, the host structural change can be coupled with the guest conformational variations, which results in the fluorescence detection of specific gases and their pressures without any chemical interaction or energy transfer. We believe that the new strategy shown here—a reporter molecule in a dynamic space—should contribute to the creation of a variety of advanced adsorbate detectors.

Methods

All reagents and chemicals were obtained from commercial sources, unless otherwise noted. The host PCP $[Zn_2(terephthalate)_2(triethylenediamine)]_n$ (**1**) and the guest DSB were prepared by previously described methods[32,50]. Partially deuterated DSB-d_{12} was synthesized by using benzaldehyde-d_6 and *p*-xylylene-bis(triphenylphosphonium chloride).

Introduction of DSB into nanochannels of 1. The host–guest composite **1**′ ⊃ DSB was prepared by direct encapsulation of DSB into host **1** by sublimation of DSB. Compound **1** was degassed by heating at 393 K under vacuum for 12 h. Guest-free **1** (200 mg) and DSB (140 mg) were mixed, and DSB was adsorbed into the nanochannel of **1** at 503 K for 3 h. Excess DSB was then removed under vacuum at 503 K for 3 h to obtain the composite **1**′ ⊃ DSB. Elemental analysis (%) for **1**′ ⊃ DSB. Found: C, 59.76; H, 4.36; N, 3.24 %. Calculated. for $[C_{22}H_{20}N_2O_8Zn_2]\cdot 0.81(C_{22}H_{18})$: C, 59.79; H, 4.36; N, 3.50%. The number of DSB molecules per unit cell of the host was 0.81.

Full experimental details are given in the Supplementary Information.

Received 10 March 2011; accepted 26 July 2011; published online 4 September 2011

References

1. Wolfbeis, O. S. Fiber-optic chemical sensors and biosensors. *Anal. Chem.* **74,** 2663–2677 (2002).
2. Lee, Y-E. K. & Kopelman, R. Optical nanoparticle sensors for quantitative intracellular imaging. *Wiley Interdiscip. Rev. Nanomed. Nanobiotechnol.* **1,** 98–110 (2009).
3. Dansby-Sparks, R. N. *et al.* Fluorescent-dye-doped sol–gel sensor for highly sensitive carbon dioxide gas detection below atmospheric concentrations. *Anal. Chem.* **82,** 593–600 (2010).
4. Demas, J. N., DeGraff, B. A. & Coleman, P. B. Oxygen sensors based on luminescence quenching. *Anal. Chem.* **1,** 793–800 (1999).
5. Baratto, C. *et al.* Luminescence response of ZnO nanowires to gas adsorption. *Sens. Actuat. B* **140,** 461–466 (2009).
6. Esser, B. & Swager, T. M. Detection of ethylene gas by fluorescence turn-on of a conjugated polymer. *Angew. Chem. Int. Ed.* **49,** 8872–8875 (2010).
7. de Vargas-Sansalvador, I. M. P. *et al.* Phosphorescent sensing of carbon dioxide based on secondary inner-filter quenching. *Anal. Chim. Acta* **655,** 66–74 (2009).
8. Liu, Y. *et al.* Fluorescent chemosensor for detection and quantitation of carbon dioxide gas. *J. Am. Chem. Soc.* **132,** 13951–13953 (2010).
9. Gerasimchuk, N., Esaulenko, A. N., Dalley, K. N. & Moore, C. 2-Cyano-2-isonitrosoacetamide and its Ag(I) complexes. Silver(I) cyanoximateas a non-electric gas sensor. *Dalton Trans.* **39,** 749–764 (2010).
10. Yaghi, O. M. *et al.* Reticular synthesis and the design of new materials. *Nature* **423,** 705–714 (2003).
11. Kitagawa, S., Kitaura, R. & Noro, S-i. Functional porous coordination polymers. *Angew. Chem. Int. Ed.* **43,** 2334–2375 (2004).
12. Bradshaw, D., Claridge, J. B., Cussen, E. J., Prior, T. J. & Rosseinsky, M. J. Design, chirality, and flexibility in nanoporous molecule-based materials. *Acc. Chem. Res.* **38,** 273–282 (2005).
13. Férey, G. Hybrid porous solids: Past, present, future. *Chem. Soc. Rev.* **37,** 191–214 (2008).
14. Murray, L. J., Dincă, M. & Long, J. R. Hydrogen storage in metal-organic frameworks. *Chem. Soc. Rev.* **38,** 1294–1314 (2009).
15. Xiao, B. *et al.* Chemically blockable transformation and ultraselective low-pressure gas adsorption in a non-porous metal organic framework. *Nature Chem.* **1,** 289–294 (2009).
16. Chen, B. L. *et al.* A luminescent metal-organic framework with Lewis basic pyridyl sites for the sensing of metal ions. *Angew. Chem. Int. Ed.* **48,** 500–503 (2009).
17. Zacher, D., Shekhah, O., Wöll, C. & Fischer, R. A. Thin films of metal-organic frameworks. *Chem. Soc. Rev.* **38,** 1418–1429 (2009).
18. McKinlay, A. C. *et al.* BioMOFs: Metal-organic frameworks for biological and medical applications. *Angew. Chem. Int. Ed.* **49,** 6260–6266 (2010).
19. Vaidhyanathan, R. *et al.* Direct observation and quantification of CO_2 binding within an amine-functionalized nanoporous solid. *Science* **330,** 650–653 (2010).
20. Xie, Z., Ma, L., deKrafft, K. E., Jin, A. & Lin, W. Porous phosphorescent coordination polymers for oxygen sensing. *J. Am. Chem. Soc.* **132,** 922–923 (2010).
21. Rabone, J. *et al.* An adaptable peptide-based porous material. *Science* **329,** 1053–1057 (2010).
22. Sato, H., Matsuda, R., Sugimoto, K., Takata, M. & Kitagawa, S. Photoactivation of a nanoporous crystal for on-demand guest trapping and conversion. *Nature Mater.* **9,** 661–666 (2010).
23. Meek, S. T., Greathouse, J. A. & Allendorf, M. D. Metal-organic frameworks: A rapidly growing class of versatile nanoporous materials. *Adv. Mater.* **23,** 249–267 (2011).
24. Choi, H. J., Dincă, M. & Long, J. R. Broadly hysteretic H_2 adsorption in the microporous metal-organic framework Co(1,4-benzenedipyrazolate). *J. Am. Chem. Soc.* **130,** 7848–7850 (2008).
25. Férey, G. & Serre, C. Large breathing effects in three-dimensional porous hybrid matter: Facts, analyses, rules and consequences. *Chem. Soc. Rev.* **38,** 1380–1399 (2009).
26. Li, J-R., Kuppler, R. J. & Zhou, H-C. Selective gas adsorption and separation in metal-organic frameworks. *Chem. Soc. Rev.* **38,** 1477–1504 (2009).
27. Muraoka, T., Kinbara, K. & Aida, T. Mechanical twisting of a guest by a photoresponsive host. *Nature* **440,** 512–515 (2006).
28. Llewellyn, P. L., Bourrelly, S., Serre, C., Filinchuk, Y. & Férey, G. How hydration drastically improves adsorption selectivity for CO_2 over CH_4 in the flexible chromium terephthalate MIL-53. *Angew. Chem. Int. Ed.* **45,** 7751–7754 (2006).
29. Oelkrug, D. *et al.* Towards highly luminescent phenylene vinylene films. *Synth. Met.* **83,** 231–237 (1996).
30. Oelkrug, D. *et al.* Tuning of fluorescence in films and nanoparticles of oligophenylenevinylenes. *J. Phys. Chem. B* **102,** 1902–1907 (1998).

31. Gierschner, J. *et al.* Solid-state optical properties of linear polyconjugated molecules: π-stack contra herringbone. *J. Chem. Phys.* **123,** 144914 (2005).
32. Dybtsev, D. N., Chun, H. & Kim, K. Rigid and flexible: A highly porous metal-organic framework with unusual guest-dependent dynamic behavior. *Angew. Chem. Int. Ed.* **43,** 5033–5036 (2004).
33. Müller, M., Devaux, A., Yang, C-H., De Cola, L. & Fischer, R. A. Highly emissive metal-organic framework composites by host-guest chemistry. *Photochem. Photobiol. Sci.* **9,** 846–853 (2010).
34. Furuya, K., Kawato, K., Yokoyama, H., Sakamoto, A. & Tasumi, M. Molecular distortion of *trans*-stilbene and the Raman intensity of the in-phase CH out-of-plane wag of the central CH = CH group. *J. Phys. Chem. A* **107,** 8251–8258 (2003).
35. Kasha, M., Rawls, H. R. & El-Bayoumi, M. A. The exciton model in molecular spectroscopy. *Pure Appl. Chem.* **11,** 371–392 (1965).
36. An, B-K., Kwon, S-K., Jung, S-D. & Park, S. Y. Enhanced emission and its switching in fluorescent organic nanoparticles. *J. Am. Chem. Soc.* **124,** 14410–14415 (2002).
37. Choi, H-S. & Suh, M. P. Highly selective CO_2 capture in flexible 3D coordination polymer networks. *Angew. Chem. Int. Ed.* **48,** 6865–6869 (2009).
38. Kanoh, H. *et al.* Elastic layer-structured metal organic frameworks (ELMS). *J. Colloid Interface Sci.* **334,** 1–7 (2009).
39. Nakagawa, K. *et al.* Enhanced selectivity of CO_2 from a ternary gas mixture in an interdigitated porous framework. *Chem. Commun.* **46,** 4258–4260 (2010).
40. Swiatkowski, G., Menzel, R. & Rapp, W. Hindrance of the rotational relaxation in the excited singlet-state of biphenyl and *para*-terphenyl in cooled solutions by methyl substituents. *J. Lumin.* **37,** 183–189 (1987).
41. Matsuda, R. *et al.* Highly controlled acetylene accommodation in a metal-organic microporous material. *Nature* **436,** 238–241 (2005).
42. Samsonenko, D. G. *et al.* Microporous magnesium and manganese formates for acetylene storage and separation. *Chem. Asian J.* **2,** 484–488 (2007).
43. Zhang, J-P. & Kitagawa, S. Supramolecular isomerism, framework flexibility, unsaturated metal center, and porous property of Ag(I)/Cu(I) 3,3′,5,5′-tetrametyl-4,4′-bipyrazolate. *J. Am. Chem. Soc.* **130,** 907–917 (2008).
44. Fischer, M., Hoffmann, F. & Fröba, M. New microporous materials for acetylene storage and C_2H_2/CO_2 separation: Insights from molecular simulations. *ChemPhysChem* **11,** 2220–2229 (2010).
45. Yanai, N. *et al.* End-functionalization of a vinylidene fluoride oligomer in coordination nanochannels. *J. Mater. Chem.* **21,** 8021–8025 (2011).
46. Löwe, C. & Weder, C. Oligo(*p*-phenylene vinylene) excimers as molecular probes: Deformation-induced color changes in photoluminescent polymer blends. *Adv. Mater.* **14,** 1625–1629 (2002).
47. Mutai, T., Satou, H. & Araki, K. Reproducible on–off switching of solid-state luminescence by controlling molecular packing through heat-mode interconversion. *Nature Mater.* **4,** 685–687 (2005).
48. Hong, Y. N., Lam, J. W. Y. & Tang, B. Z. Aggregation-induced emission: Phenomenon, mechanism and applications. *Chem. Commun.* 4332–4353 (2009).
49. van Hutten, P. F., Krasnikov, V. V., Brouwer, H-J. & Hadziioannou, G. Excimer luminescence from single crystals and films of a cyano-substituted phenylene-vinylene model compound. *Chem. Phys.* **241,** 139–154 (1999).
50. Campbell, T. W. & Mcdonald, R. N. Synthesis of hydrocarbon derivatives by the Wittig synthesis. I. Distyrylbenzenes. *J. Org. Chem.* **24,** 1246–1251 (1959).

Acknowledgements

This work was supported by the Murata Science Foundation, ERATO-JST, a Grant-in-Aid for Young Scientists (A), and a Grant-in-Aid for Scientific Research on Innovative Area 'Emergence in Chemistry' from MEXT. The synchrotron radiation experiments were carried out at BL02B2 in SPring-8 with the approval of the Japan Synchrotron Radiation Research Institute (JASRI) (Proposal no. 2009B1320).

Author contributions

N.Y., K.K., and T.U. designed and carried out the experiments. Y.H. performed the density functional calculations. H.S. and R.M. performed *in-situ* infrared and Raman measurements. Y.K. and M.T. assisted with the *in situ* synchrotron XRPD measurements and carried out the Le Bail fitting analysis of the XRPD data. M.M. contributed ^{2}H NMR measurements. N.Y., K.K., T.U., and S.K. wrote the manuscript.

Additional information

The authors declare no competing financial interests. Supplementary information accompanies this paper on www.nature.com/naturematerials. Reprints and permissions information is available online at http://www.nature.com/reprints. Correspondence and requests for materials should be addressed to T.U. or S.K.